

# A Study of Heavy Higgs Properties at a Multi-TeV $e^+e^-$ Collider

Marco Battaglia<sup>1,2,3</sup>, Frederik Bogert<sup>1</sup>, Arnaud Ferrari<sup>4</sup>, Johan Relefors<sup>4</sup> and Sarah Zalusky<sup>1</sup>

1- University of California at Santa Cruz - Santa Cruz Institute of Particle Physics,  
Santa Cruz, CA 95064 - USA

2- Lawrence Berkeley National Laboratory, Berkeley, CA 94720 - USA

3- CERN, CH-1211 Geneva - Switzerland

4- Uppsala University - Department of Physics and Astronomy, 75120 Uppsala - Sweden

The precise determination of the masses of the neutral and charged heavy Higgs bosons is a crucial input for the study of Supersymmetry and its relation with cosmology through dark matter. This paper presents a study of  $e^+e^- \rightarrow H^0A^0$  and  $H^+H^-$  production at  $\sqrt{s}=3$  TeV. The analysis is performed with full simulation and reconstruction accounting for beamstrahlung effects and the overlay of  $\gamma\gamma \rightarrow$  hadrons events. Results are presented in terms of the accuracy on the determination of the masses and widths of the heavy Higgs bosons in two benchmark scenarios.

## 1 Introduction

The precise determination of the masses and widths of the neutral and charged heavy Higgs bosons is an important part of the study of an extended Higgs sector in models of new physics. A non-minimal Higgs sector is one of the simplest extension of the Standard Model (SM), realised in the Two Higgs Doublet Model, which acquires a special relevance and justification in supersymmetric models. In Supersymmetry the detailed study of the heavy Higgs sector is crucial to assess the relation between new physics and cosmology, through dark matter [1]. A high-energy lepton collider is particularly well suited for such a study even in those regions of the parameter space where the sensitivity of the LHC becomes marginal. In particular, the pair production processes,  $e^+e^- \rightarrow H^0A^0$  and  $e^+e^- \rightarrow H^+H^-$  give access to all four heavy Higgs states almost up to the kinematical limit [2–4].

## 2 Simulation

In this benchmark study we consider two SUSY models with  $M_A = 742$  GeV and 902 GeV, respectively, at  $\sqrt{s} = 3$  TeV and adopt the proposed CLIC beam parameters. The model parameters and the masses of the relevant particles are given in Table 1. The cross sections for  $e^+e^- \rightarrow H^0A^0$  and  $e^+e^- \rightarrow H^+H^-$  pair production are given in Table 2. The properties of the heavy Higgs sector are largely independent on the details of supersymmetric models and chosen mostly depend on the values of  $M_A$  and  $\tan\beta$ . It is interesting to observe that the chosen values of these parameters are compatible with the current LHC data and with a  $\sim 125$  GeV lightest supersymmetric Higgs boson,  $h^0$ , in the general MSSM. In particular, the scenario 1 is compatible with a non-observation of SUSY signals in the channels with missing transverse energy by the end of the 8 TeV LHC run and  $123 < M_h < 127$  GeV in the MSSM [5]. Signal events are generated with *Isasugra* 7.69 [6] and *Pythia* 6.215 [7]. Taking into account the CLIC luminosity spectrum, the predicted signal cross sections for  $H^0A^0$  and  $H^+H^-$  are respectively 0.7 (0.4) fb and 1.6 (1.1) fb in the scenario 1 (2). The

Table 1: Model parameters and Higgs boson masses of the two benchmark points studied.

	Scenario 1	Scenario 2
Mass Parameters (GeV)	$M_1 = 780$ $M_2 = 940$ $M_3 = 540$	$m_0 = 800$ $m_{1/2} = 966$
$\tan\beta$ , $A_0$ , $\text{sign}(\mu)$	24, -750, +	51, 0, -
$M_A$ , $M_{H^0}$ , $M_{H^\pm}$ (GeV)	902.6, 902.4, 906.3	742.8, 742.0, 747.6

dominant decay modes are  $H^0 \rightarrow b\bar{b}$ ,  $A^0 \rightarrow b\bar{b}$  and  $H^\pm \rightarrow t\bar{b}$  leading to the  $b\bar{b}b\bar{b}$  and  $t\bar{b}t\bar{b}$  final states. The main SM background processes are generated with `Pythia 6.215` and `WHIZARD`.

Table 2: Summary of the processes considered in this study with their production cross section and the event generator used.

Process	$\sigma$ (fb)	Generator
$H^0 A^0$	0.7 / 0.4	ISASUGRA 7.69+PYTHIA 6.215
$H^+ H^-$	1.6 / 1.1	ISASUGRA 7.69+PYTHIA 6.215
Inclusive SUSY	84.9 / 77.1	ISASUGRA 7.69+ PYTHIA 6.215
$W^+ W^-$	728.2	PYTHIA 6.215
$Z^0 Z^0$	54.8	PYTHIA 6.215
$t\bar{t}$	30.2	PYTHIA 6.215
$b\bar{b}b\bar{b}$	5.8	WHIZARD
$W^+ W^- Z^0$	32.8	CompHEP+PYTHIA 6.215
$Z^0 Z^0 Z^0$	0.5	CompHEP+PYTHIA 6.215

In addition, the irreducible inclusive  $b\bar{b}b\bar{b}$  SM background is generated with `CompHep` [8] at the parton level and subsequently hadronised with `Pythia`. We assume the beams to be unpolarised. Events are processed through full detector simulation using the `Geant-4`-based `Mokka` [9] program and reconstructed with `Marlin`-based [10] processors assuming a version of the ILD detector [11], modified for physics at CLIC. Particle tracks are reconstructed by the combination of a Time Projection Chamber and a pixellated Si Vertex Tracker. The momentum resolution is  $\delta p/p^2 = 2 \times 10^{-5} \text{ GeV}^{-1}$  and the impact parameter resolution is  $\sigma_{R-\phi} = (2.5 \oplus \frac{21}{p_t(\text{GeV})}) \mu\text{m}$ . The parton energy is reconstructed using the `Pandora` particle flow algorithm [12]. Performances for our signal events are discussed in the next session. For the  $\gamma\gamma \rightarrow$  hadrons background simulation two-photon events are generated with the `Guinea Pig` program [13] using the nominal CLIC CDR beam parameters at  $\sqrt{s} = 3 \text{ TeV}$  where the hadronic background cross section is modelled following [14]. The energies of two colliding photons are stored with their corresponding probability and passed to `Pythia` for the generation of the hadronic events. On average, there are 3.3  $\gamma\gamma \rightarrow$  hadrons events per bunch crossing (BX) with  $M_{\gamma\gamma} > 3 \text{ GeV}$ . These are passed through the same `Mokka` full detector simulation and overlaid to the particles originating from the primary  $e^+e^-$  interaction at the reconstruction stage, using the event overlay feature in the `lcio` persistency package [15]. For this analysis, the  $\gamma\gamma$  background is overlaid only to the signal  $H^0 A^0$  and  $H^+ H^-$  events, in order to study its effect on the signal reconstruction and to the peaking background from the cross-feed of  $H^+ H^-$  events in the  $H^0 A^0$  analysis and vice

versa.

### 3 Event Reconstruction and Signal Selection

The event reconstruction and selection is based on the identification of four heavy parton final states in spherical events with large visible energy and equal di-parton invariant masses. Details of the  $bbbb$  analysis can be found in [4]. Most of the analysis criteria are common to both the  $bbbb$  and the  $tbtb$  channels. The analysis starts with a cut-based event pre-selection. Jet clustering is applied to pre-selected events, followed by  $b$  and  $t$  identification. A kinematic fitting is performed to improve the di-jet invariant mass resolution, mitigate the impact of machine-induced backgrounds on the parton energy resolution and reject remaining physics backgrounds.

In order to reject particles which are poorly reconstructed or likely to originate from underlying  $\gamma\gamma$  events, a set of minimal quality cuts are applied. Only particles with transverse momentum  $p_t > 0.95$  GeV are considered, charged particles are also required to have at least 12 hits in the tracking detectors and relative momentum uncertainty  $\delta p/p < 1$ . The event selection proceeds as follows. First multi-jet hadronic events with large visible energy are selected. We require events to have at least 50 charged particles, total reconstructed energy exceeding 2.3 TeV, event thrust between 0.62 and 0.91, sphericity larger than 0.04 and smaller than 0.75, transverse energy exceeding 1.3 TeV and  $3 \leq N_{\text{jets}} \leq 5$ , where  $N_{\text{jets}}$  is the natural number of jets reconstructed using the Durham clustering algorithm [16] with  $y_{\text{cut}}=0.0025$ . These cuts remove all the SUSY events with missing energy and the  $e^+e^- \rightarrow f\bar{f}$  events. For events fulfilling these criteria, we perform the final jet reconstruction using the anti-kt clustering algorithm in cylindrical coordinates [17], implemented in the **FastJet** package, ported as a custom processor in the **Marlin** analysis framework. The choice of cylindrical coordinates is optimal since the  $\gamma\gamma \rightarrow$  hadrons events are forward boosted, similarly to the underlying events in  $pp$  collisions at the LHC, for which the anti-kt clustering has been conceived and optimised. For each event, the minimum  $R$  value at which the event has exactly four jets with energies in excess of 150 GeV is used for the clustering. The di-jet invariant mass is computed from pairing these jets. Since there are three possible permutations for pairing the four energetic jets and the pair-produced bosons are expected to be (almost) degenerate in mass, we take the combination minimising the difference  $\Delta M$  of the two di-jet invariant masses and require  $|\Delta M| < 160$  GeV, 150 GeV for the  $H^0 A^0$  and  $H^+ H^-$ , respectively. Since the signal events are predominantly produced in the central region while the  $\gamma\gamma$  events and most of the SM background processes are forward peaked, we only accept events for which the jet with the minimum polar angle,  $\theta$ , has  $|\cos\theta| < 0.92$ . The single most effective event selection to separate signal events from the SM backgrounds is  $b$ -tagging, since the signal contains four  $b$  hadrons. The irreducible SM  $b\bar{b}b\bar{b}$  background has a cross section of only 0.5 fb and is effectively reduced by the equal di-jet mass constrain and kinematic fitting. The  $b$ -tagging procedure is based on the response of the vertexing variables of the ZVTOP program [18]. This uses the kinematics and topology of the secondary particles in the jet. For this analysis, the vertex variables are supplemented by the corresponding kinematic observables for the secondary system reconstructed based on the charged particle impact parameters instead of the topological vertexing, when ZVTOP does not return any secondary vertex. This procedure increases the efficiency for  $b$  jets at the higher end of the kinematic spectrum in signal events. Tagging observables are combined into a single discriminating variable using the boosted decision tree method with the TMVA

package [19]. In the case of charged Higgs bosons, top tagging is also performed. First the event is reconstructed as a four jet event and jets are tested for their compatibility with the top mass. Then a de-clustering procedure is applied to the jets to study possible jet substructure arising from the  $t \rightarrow Wb \rightarrow q\bar{q}'b$  decay. This follows the procedure originally developed for identifying highly boosted top quarks at the LHC [20, 21].

In order to improve the di-jet mass resolution, we apply a constrained kinematic fit. We use the port of the `Pufitc` kinematic fit algorithm [22] to the MARLIN framework. `Pufitc` was originally developed for  $W^+W^-$  reconstruction in DELPHI at LEP-2 and it has been successfully applied for the reconstruction of simulated linear collider events at lower energies [3]. The kinematic fit adjusts the momenta of the four jets as  $p_F = ap_M + bp_B + cp_C$ , where  $p_M$  is the jet momentum from particle flow,  $p_B$  and  $p_C$  are unit vectors transverse to  $p_M$  and to each other,  $a$ ,  $b$  and  $c$  free parameters. For these analyses, we impose the constraints  $p_x = p_y = 0$ ,  $E \pm |p_z| = \sqrt{s}$  and  $M_{jj1} = M_{jj2}$ , where the second condition accounts for beamstrahlung photons radiated along the beam axis. We only accept events with a kinematic fit  $\chi^2 < 5$ . After the kinematic fit, the relative jet energy resolution  $\text{RMS}_{90}/E_{\text{jet}}$  for  $b$  jets is  $0.075 \pm 0.002$  and  $0.096 \pm 0.002$  without and with  $\gamma\gamma$  background overlaid, respectively. The use of a kinematic fit also mitigates the effect of the overlaid  $\gamma\gamma$  events on the di-jet mass resolution. Since we do impose the nominal centre-of-mass energy, allowing for beamstrahlung, jet energies are rescaled in the fit to be consistent with that of  $\sqrt{s}$ . The di-jet invariant mass resolution changes from  $(38 \pm 4)$  GeV, for the raw particle flow objects, to  $(29 \pm 3)$  GeV, using the kinematic fit, and to  $(18 \pm 2)$  GeV, imposing the equal mass constrain, in absence of  $\gamma\gamma$  background. Using the kinematic fit and equal mass constrain we obtain  $(19.3 \pm 3.0)$  GeV with the  $\gamma\gamma$  background overlaid. The use of the equal mass constrain is justified in the case of the  $e^+e^- \rightarrow H^0A^0$  channel in SUSY models. In fact, the mass splitting between the  $A^0$  and  $H^0$  bosons is always smaller than both the natural widths and the experimental di-jet mass resolution, in particular in the region of MSSM parameters where their determination is most crucial to fix the relic dark matter density  $\Omega_\chi h^2$ . This has been verified through a dedicated study using `FeynHiggs` [23]. The few cases in which the mass splitting becomes large are also characterised by very large natural widths of the two bosons.

## 4 Results

The di-jet invariant mass distributions for the  $b\bar{b}b\bar{b}$  and  $t\bar{b}t\bar{b}$  final states are shown in Figure 1.

The masses and widths of the heavy bosons are extracted from a multi-parameter fit to

Table 3: Summary of the fit results for the masses and widths for benchmark scenario 1, without and with  $\gamma\gamma$  background overlay. The quoted uncertainties are statistical only.

	State	Mass (GeV)	Width (GeV)
No $\gamma\gamma$	$A^0/H^0$	$742.7 \pm 1.4$	$21.7 \pm 3.3$
No $\gamma\gamma$	$H^\pm$	$744.3 \pm 2.0$	$17.0 \pm 4.7$
$\gamma\gamma$ (20 BX)	$A^0/H^0$	$743.7 \pm 1.7$	$22.2 \pm 3.8$
$\gamma\gamma$ (20 BX)	$H^\pm$	$746.9 \pm 2.1$	$21.4 \pm 4.9$

Table 4: Summary of the fit results for the masses and widths for benchmark scenario 2, without and with  $\gamma\gamma$  background overlay. The quoted uncertainties are statistical only.

	State	Mass (GeV)	Width (GeV)
No $\gamma\gamma$	$A^0/H^0$	$902.1 \pm 1.9$	$21.4 \pm 5.0$
No $\gamma\gamma$	$H^\pm$	$901.4 \pm 1.9$	$18.9 \pm 4.4$
$\gamma\gamma$ (20 BX)	$A^0/H^0$	$904.5 \pm 2.8$	$20.6 \pm 6.3$
$\gamma\gamma$ (20 BX)	$H^\pm$	$902.6 \pm 2.4$	$20.2 \pm 5.4$

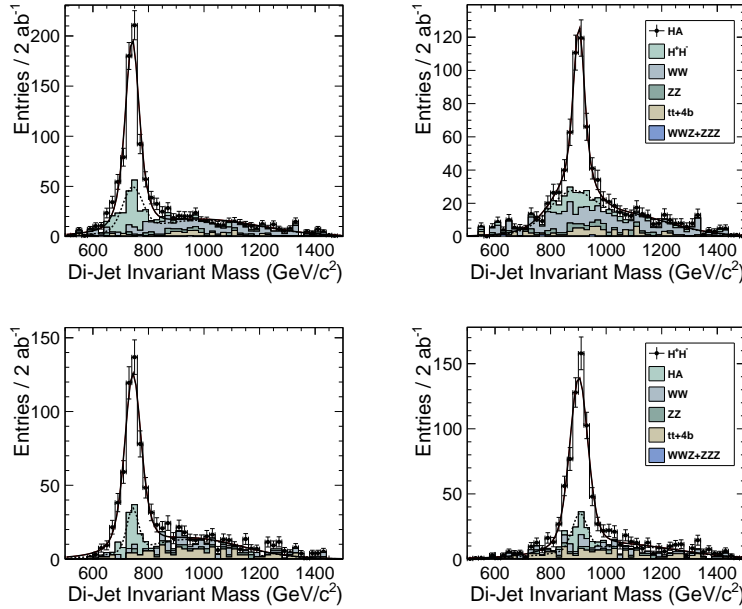


Figure 1: Di-jet invariant mass distribution of fully simulated and reconstructed events in the channel  $e^+e^- \rightarrow b\bar{b}b\bar{b}$  (upper row) and  $e^+e^- \rightarrow t\bar{t}b\bar{b}$  (lower row). The contributions from the different processes are shown. The dotted line shows the fitted background distribution which includes the peaking contribution of the cross feeds from the  $H^0A^0$  and  $H^+H^-$  processes. The continuous line shows the global fit including the signal.

these distributions. In order to assess the effect of the  $\gamma\gamma \rightarrow$  hadrons background on the accuracy of the mass and width reconstruction, we repeat the analysis assuming first no  $\gamma\gamma$  background and then we overlay the background assuming an effective 10 ns time stamping capability of the detector, corresponding to the integration of 20 bunch crossings (BX). Results are summarised in Tables 3 and 4.

We observe that the heavy Higgs mass can be measured to a relative statistical accuracy of better than 0.5%. This accuracy is preserved in the presence of  $\gamma\gamma$  background by applying the anti-kt jet clustering and kinematic fitting, provided the global detector stamping resolution is  $\leq 10$  ns. The width can be measured to a relative accuracy of 0.20-0.30. These

measurements are important both for constraining the model parameters through  $M_A$  and  $\tan\beta$  and for assessing the contribution of the  $\tilde{\chi}^0\tilde{\chi}^0 \rightarrow A^0 \rightarrow b\bar{b}$  pole annihilation process in setting the relic dark matter density in the Universe [1]. These accuracies ensures that the heavy Higgs mass contribution to the statistical precision in the extraction of  $\Omega_\chi h^2$  in a generic MSSM model, with dark matter annihilation through the  $A^0$  pole, is of order of 0.10. In the specific case of scenario 2, where  $\tan\beta$  is large and  $M_A=742$  GeV, these constraints on  $\Gamma_{A^0}$  and  $\Gamma_{H^\pm}$  also yield a relative statistical accuracy on the determination of  $\tan\beta$  to  $\sim 0.20$ .

## 5 Conclusions

A study of  $H^0A^0$  and  $H^+H^-$  production in  $\sqrt{s} = 3$  TeV  $e^+e^-$  collisions performed on fully simulated and reconstructed events with realistic backgrounds shows that the mass and widths of these bosons can be determined with a relative accuracy of 0.05 and 0.2-0.30, respectively, provided time stamping with a resolution  $\leq 10$  ns can be achieved in the detector.

## References

- [1] E. A. Baltz, M. Battaglia, M. E. Peskin and T. Wizansky, Phys. Rev. D **74** (2006) 103521 [hep-ph/0602187].
- [2] E. Coniavitis, A. Ferrari, Phys. Rev. **D75** (2007) 015004.
- [3] M. Battaglia, B. Hooberman, N. Kelley, Phys. Rev. D **78** (2008) 015021.
- [4] M. Battaglia and P. Ferrari, CERN LCD Note-2010-006, arXiv:1006.5659 [hep-ex].
- [5] A. Arbey, M. Battaglia and F. Mahmoudi, to appear on Eur. Phys. J. C, arXiv:1112.3032 [hep-ph].
- [6] F. E. Paige, S. D. Protopopescu, H. Baer and X. Tata, arXiv:hep-ph/0312045.
- [7] T. Sjostrand, S. Mrenna and P. Z. Skands, JHEP **0605** (2006) 026 [arXiv:hep-ph/0603175].
- [8] E. Boos *et al.* [CompHEP Collaboration], Nucl. Instr. and Meth. A **534** (2004), 250.
- [9] P. Mora de Freitas, in Proc. of the *Int. Conf. on Linear Colliders (LCWS 04)*, Ed. de l'Ecole Polytechnique, Paris, 2004, vol. I, 437.
- [10] F. Gaede, Nucl. Instrum. Meth. A **559** (2006) 177.
- [11] H. Stoeck *et al.* [The ILD Concept Group], The International Large Detector - Letter of Intent, March 2009.
- [12] M. A. Thomson, Nucl. Instrum. Meth. A **611** (2009) 25 [arXiv:0907.3577 [physics.ins-det]].
- [13] D. Schulte, TESLA Note 97-08.  
The  $\gamma\gamma$  events have been generated by Daniel Schulte.
- [14] G. A. Schuler and T. Sjöstrand, CERN-TH/96-119.
- [15] F. Gaede, T. Behnke, R. Cassell, N. Graf, T. Johnson and H. Vogt, in Proc. of *Computing in high energy physics and nuclear physics*, Interlaken, 2004, 471.
- [16] S. Catani, Y. L. Dokshitzer, M. Olsson, G. Turnock and B. R. Webber, Phys. Lett. B **269** (1991) 432.
- [17] M. Cacciari, G. P. Salam and G. Soyez, JHEP **0804** (2008) 063 [arXiv:0802.1189 [hep-ph]].
- [18] D. Bailey *et al.* [LCFI Collaboration], Nucl. Instrum. Meth. A **610** (2009) 573 [arXiv:0908.3019 [physics.ins-det]].
- [19] A. Hocker, J. Stelzer, F. Tegenfeldt *et al.*, PoS ACAT (2007) 040 [physics/0703039 [PHYSICS]].
- [20] D. Kaplan *et al.*, arXiv:0806.0848 [hep-ph].
- [21] The CMS Collaboration, CMS PAS JME-09-011.
- [22] P. Abreu *et al.* [DELPHI Collaboration] Eur. Phys. J. C **2** (1998) 581.
- [23] T. Hahn, S. Heinemeyer, W. Hollik, H. Rzehak and G. Weiglein, Comput. Phys. Commun. **180** (2009) 1426.